# Energetic Macroscopic Representation-based scaling laws of PMSM for electric vehicles simulations

Ayoub Aroua[a,b], Walter Lhomme[a,*], Florian Verbelen[b,c], Alain Bouscayrol[a], Peter Sergeant[b,c] & Kurt Stockman[b,c]

[a] *Univ. Lille, Arts et Metiers Institute of Technology, Centrale Lille, Junia, ULR 2697 – L2EP, F-59000 Lille, France*

[b] *Department of Electromechanical, Systems and Metal Engineering, Ghent University, Belgium*

[c] *Flanders Make@UGent – core lab* Miro, *Belgium*

**Abstract** – **The paper presents a method for structuring a scalable model of a permanent magnet synchronous machine in a manner that facilitates its integration into system-level simulations. This is achieved by utilizing the energetic macroscopic representation formalism to organize the equations of the scaling laws. The model comprises a fixed reference permanent magnet synchronous machine model that is complemented with two electrical and mechanical power adaptation elements to ensure scalability. Three scaling choices are analyzed, and the findings reveal that the equations for the power adaptation elements differ based on the selected scaling choice.**

**Keywords— Energetic Macroscopic Representation, electric machine scaling, scaling factors, scalable models**

## 1. INTRODUCTION

A Permanent Magnet Synchronous Machine (PMSM) is a key component of the powertrain of electric vehicles [1]. This latter needs to address the requirement of a broad range of automotive applications. To speed up the design of PMSM scaling laws have received considerable attention in research studies [2]. Scaling laws enable the assessment of a new design of varying dimensions, based on this pre-existing design. These laws furnish a methodology for comprehending the influence of altering representative parameters of a reference design, to derive a scaled component with distinct specifications. The advantage of these scaling laws is the simplicity of the method and the fact that they can be applied at early design stages. The scaling laws are derived based on three scaling factors, namely axial, radial, and rewinding. On top of that, the derivation of these scaling laws depends on a choice that is made at the beginning of the scaling process. For instance, Stipetic et *al.* in derived scaling laws based the conservation of the magnetic field density and saturation level $B\sim1$ [3]. Borisavljevic *et al.* investigated scaling laws by preserving the same heating $\Theta\sim1$, (power loss-to-cooling surface ratio) [4]. Multon et *al.* examined scaling laws by making a hybrid choice of the two first ones [5].

For ease of integration at system-level simulations of the scaling laws, a new organization of the scaled PMSM is proposed in [6]. The equations are reorganized by keeping a reference PMSM model fixed, but complemented with two electrical and mechanical power adaptation elements. The novel aspect of this approach is the incorporation of scaling laws within the power adaptation elements, which enables scalability by adjusting the input and output variables of the reference model. The new model structuration is achieved using Energetic Macroscopic Representation (EMR) formalism [7]. By implementing the new scalable model of PMSM in the powertrain model of an electric vehicle, it is possible to analyze the performance of a broad range of vehicles.

The scalable model in [6] is deduced based on one single scaling choice, which consists of preserving the magnetic field density. The objective of this paper is to extend the presented work in the aforementioned reference to consider different scaling choices of PMSM. The remainder of the paper is organized as follows. Section 2 presents the scaling laws for PMSM. The EMR-based scaling laws are discussed in Section 3. Section 4 is dedicated to the results and discussion. The emphasis is placed on analyzing the losses and efficiency of the scaled PMSM with a specific focus on the power adaptation elements.

## 2. SCALING LAWS OF PMSM

To scale a PMSM, the scaling process implies three procedures: axial, radial, and rewinding. The axial scaling procedure consists of altering the core length of the machine using an axial scaling factor $K_{\mathrm{A}}$. The radial scaling consists of proportionally altering the geometrical parameters of the cross-section with a radial scaling factor $K_{\mathrm{R}}$. The rewinding scaling is used to adjust the voltage of the scaled machine to the predefined inverter voltage limit using a rewinding scaling factor $K_{\mathrm{W}}$. Based on these scaling factors, scaling laws for the machine properties (e.g. voltage, torque, power, losses…) as well as the machine parameters (e.g. resistance, inductance, inertia…) can be deduced. It is necessary to make a selection of variables to maintain constant during the scaling process. The choice of these constant variables will significantly influence the results of the scaling laws.

Table 1 presents the scaling laws of some key parameters of PMSM according to the aforementioned choices and as a function of the scaling factors.

## 3. EMR-BASED SCALING LAWS

According to [6], the concept is to incorporate Power Adaptation (PA) elements on both the electrical and mechanical sides of the PMSM reference model (Fig. 1). These PA are used to scale the inputs and outputs of the reference model. The challenge is therefore to define the equations for the PA elements, which considers the three scaling factors, the scaling choices, and the different scaled losses. The proposed organization is defined according to the EMR rules.

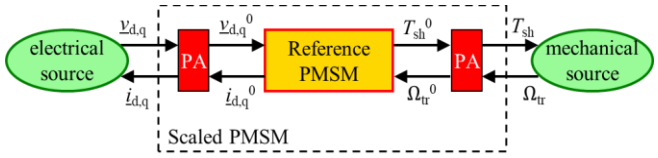


Fig. 1: Proposed structural methodology of the scaled PMSM

Table 1: Scaling laws of the quantities of PMSM according to the scaling choice. $K_A$, $K_R$, *and* $K_W$ refers to axial, radial, and rewinding scaling factors, respectively

| | $B\sim1$ | $\Theta\sim1$ | Hybrid choice |
|---|---|---|---|
| Current density $J$ [A/mm$^2$] | $1/K_R$ | $1/\sqrt{K_R}$ | $1/\sqrt{K_R}$ |
| Magnetic field density $B$ [T] | 1 | $1/\sqrt{K_R}$ | 1 |
| Electromagnetic torque $T_{EM}$ [Nm] | $K_A K_R^2$ | $K_A K_R^2$ | $K_A K_R^{2.5}$ |
| Current $i$ [A] | $\frac{K_R}{K_W}$ | $\frac{K_R^{1.5}}{K_W}$ | $\frac{K_R^{1.5}}{K_W}$ |
| Flux linkage $\psi$ [Wb] | $K_A K_R K_W$ | $K_A K_R^{0.5} K_W$ | $K_A K_R K_W$ |
| Core resistance $R_{co}$ [Ω] | $\frac{K_W^2 K_A}{K_R^2}$ | $\frac{K_W^2 K_A}{K_R^2}$ | $\frac{K_W^2 K_A}{K_R^2}$ |
| End-winding resistance $R_{ew}$ [Ω] | $\frac{K_W^2}{K_R}$ | $\frac{K_W^2}{K_R}$ | $\frac{K_W^2}{K_R}$ |
| Copper loss (active part) [W] | $K_A$ | $K_A K_R$ | $K_A K_R$ |
| Copper loss (end winding part) | $K_R$ | $K_R^2$ | $K_R^2$ |
| Permanent magnet loss [W] | $K_A K_R^4$ | $K_A K_R^3$ | $K_A K_R^4$ |
| Iron loss [W] | $K_A K_R^2$ | $K_A K_R$ | $K_A K_R^2$ |
| Inertia [kg m$^2$] | $K_A K_R^4$ | $K_A K_R^4$ | $K_A K_R^4$ |

### 3.1. *Reference PMSM*

The analysis assumes that the machine is only considered in the Park framework. The model of the reference machine (1)-(5) is represented by EMR using two elements (Fig. 2): the winding dynamic (orange rectangle pictograms with an oblique bar) and the electromagnetic conversion (orange circle pictogram). The currents $\underline{i}_{d,q}^0$ and speed $\Omega_{tr}$ are the inputs of the reference model, while the back EMF $\underline{e}_{d,q}^0$ and shaft torque $T_{sh}^0$ are its outputs. The shaft torque is determined by subtracting the equivalent iron core torque $T_{Fe}^0$ and magnet torque $T_{PM}^0$ from the electromagnetic torque $T_{em}^0$. Note that the equation numbers are recalled in EMR, which are above each pictogram in Fig. 2. In the sequel, superscript 0 refers to the variables of the reference machine.

$$\frac{d}{dt}\underline{\psi}_{d,q}^0 = \underline{v}_{d,q}^0 - (R_{co}^0 + R_{ew}^0)\underline{i}_{d,q}^0 - \underline{e}_{d,q}^0 \quad (1)$$

$$T_{em}^0 = N_p\left[\psi_d^0 i_q^0 + \psi_q^0 i_d^0\right] \quad (2)$$

$$T_{sh}^0 = T_{em}^0 - T_{Fe}^0 - T_{mag}^0 \quad (3)$$

$$\begin{cases} T_{Fe}^0 = P_{Fe}^0/\Omega_{tr} \\ T_{mag}^0 = P_{mag}^0/\Omega_{tr} \end{cases} \quad (4)$$

$$\begin{cases} e_d^0 = -N_p \Omega_{tr}^0 \psi_q^0 \\ e_q^0 = N_p \Omega_{tr}^0 \psi_d^0 \end{cases} \quad (5)$$

### 3.2. *Electrical Power Adaptation*

Making use of Table 1, the voltages $\underline{v}_{d,q}$ of the scaled machine can be expressed in a unified way for the three scaling choices as a function of the parameters of the reference machine and the scaling factors (6).

$$\underline{v}_{d,q} = K_A K_R^n K_W \frac{d}{dt}\underline{\psi}_{d,q}^0 + K_W^2\left(\frac{K_A}{K_R^2}R_{co}^0 + \frac{1}{K_R}R_{ew}^0\right)\frac{K_R^m}{K_W}\underline{i}_{d,q}^0 + K_A K_R^n K_W \underline{e}_{d,q}^0 \quad (6)$$

where n and m are exponents that are defined based on the scaling choices. The electrical PA is derived by refining (6) to get the voltages $\underline{v}_{d,q}^0$ applied to the reference model. To this end, a voltage scaling factor $K_v$ and an equivalent resistance $\Delta R^0$ is introduced (7)-(9). Furthermore, a current scaling factor $K_i$ is introduced as the ratio between the scaled and reference currents. The PA is described in EMR by an orange square pictogram with the symbol ">" inside. The sign means that the scaled PMSM power is greater than the reference PMSM power.

$$\begin{cases} \underline{v}_{d,q}^0 = (\underline{v}_{d,q}/K_v) - \Delta R^0 \underline{i}_{d,q}^0 \\ \underline{i}_{d,q} = K_i\, \underline{i}_{d,q}^0 \end{cases} \quad (7)$$

$$\Delta R^0 = \frac{1}{K_R^x}\left(\frac{R_{co}^0}{K_R} + \frac{R_{ew}^0}{K_A}\right) - R^0 \quad (8)$$

$$\begin{cases} K_v = K_A K_R^n K_W \\ K_I = \frac{K_R^m}{K_W} \end{cases} \quad (9)$$

in which x, n, and m are exponents that depend on the scaling choice and are summarized in Table 2.

Table 2: Overview of the exponents used for the power adaptation elements

| | $B\sim1$ | $\Theta\sim1$ | Hybrid choice |
|---|---|---|---|
| x in (8) | 1 | 0 | 0.5 |
| n in (9) | 1 | 0.5 | 1 |
| m in (9) | 1 | 1.5 | 1.5 |
| $\alpha$ in (11) | 2 | 2 | 2.5 |
| $\beta$ in (12) | 0 | 1 | 0.5 |
| $\gamma$ in (13) | 2 | 1 | 1.5 |

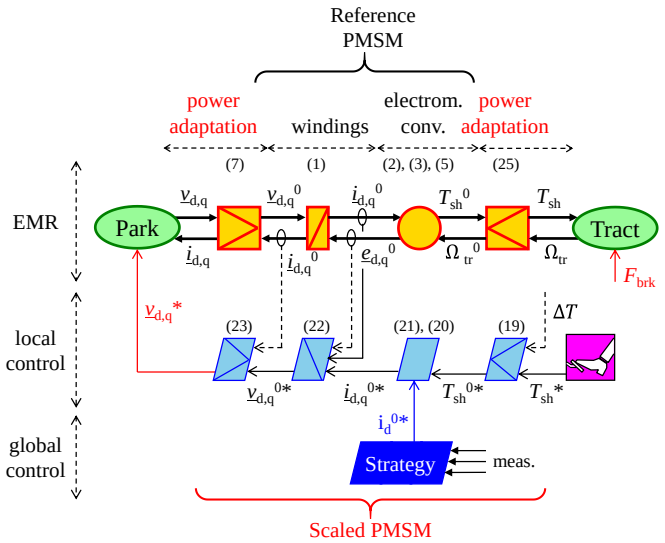


Fig. 2: EMR-based scaling laws of PMSM

### 3.3. *Mechanical Power Adaptation*

The mechanical power adaptation element is derived from (3), and the scaling factors for torque and power loss, presented in Table 1. To achieve this, the shaft torque of the reference machine $T_{sh}^0$ is scaled by a torque scaling factor, referred to $K_T$. However, since the power loss scaling factors differ from $K_T$

(see Table 1), an equivalent torque $\Delta T$ must be subtracted to find the right value of the scaled torque (11)-(13). Furthermore, it is assumed that the reference and the scaled machines operate at the same speed.

$$T_{\mathrm{sh}} = K_{\mathrm{T}} T^{0}_{\mathrm{sh}} - \Delta T \tag{10}$$

$$\begin{cases} K_{\mathrm{T}} = K_{\mathrm{A}} K_{\mathrm{R}}^{\alpha} \\ \Delta T = \Delta T_{\mathrm{fer}} + \Delta T_{\mathrm{PM}} \end{cases} \tag{11}$$

$$\Delta T_{\mathrm{fer}} = K_{\mathrm{T}} \left( \frac{1}{K_{\mathrm{R}}^{\beta}} - 1 \right) T^{0}_{\mathrm{fer}} \tag{12}$$

$$\Delta T_{\mathrm{PM}} = K_{\mathrm{T}} \left( K_{\mathrm{R}}^{\gamma} - 1 \right) T^{0}_{\mathrm{PM}} \tag{13}$$

in which $\alpha$, $\beta$, and $\gamma$ are exponents that depend on the scaling choice and are summarized in Table 2, $\Delta T_{\mathrm{fer}}$ and $\Delta T_{\mathrm{PM}}$ represent the equivalent torques for iron and magnet, respectively.

### 3.4. *Scaled losses*

Based on both electrical and mechanical PA elements, a new model organization of the losses $P_{\mathrm{loss}}$ of the scaled PMSM can be deduced, based on the power loss of the reference machine and equivalent loss terms $\Delta P$ (14)-(16).

$$P_{\mathrm{loss}} = P_{\mathrm{cu}} + P_{\mathrm{fer}} + P_{\mathrm{mag}} \tag{14}$$

$$\begin{cases} P_{\mathrm{cu}} &= K_T P^{0}_{\mathrm{cu}} + \Delta P_{\mathrm{Cu}} \\ P_{\mathrm{fer}} &= K_T P^{0}_{\mathrm{fer}} + \Delta P_{\mathrm{fer}} \\ P_{\mathrm{PM}} &= K_T P^{0}_{\mathrm{PM}} + \Delta P_{\mathrm{PM}} \end{cases} \tag{15}$$

$$\begin{cases} \Delta P_{\mathrm{Cu}} &= K_{\mathrm{T}} \Delta R^{0} \left( {i^{0}_{d}}^{2} + {i^{0}_{q}}^{2} \right) \\ \Delta P_{\mathrm{fer}} &= \Delta T_{\mathrm{fer}} \Omega^{0}_{\mathrm{tr}} \\ \Delta P_{\mathrm{PM}} &= \Delta T_{\mathrm{PM}} \Omega^{0}_{\mathrm{tr}} \end{cases} \tag{16}$$

According to the values of both axial and radial scaling factors, the equivalent loss terms $\Delta P$ can be either positive or negative. This can be observed by analyzing (8), (12), and (13). A positive value of $\Delta P$ means that the scaling process result in gearter losses than a linear losses-to-power scaling and vice versa.

The extra copper losses $\Delta P_{\mathrm{cu}}$, due to the addition of the equivalent resistance $\Delta R^{0}$, can be seen as the ratio between the electric power of the scaled and reference machine, as described in (17).

$$\Delta P_{\mathrm{cu}} = \underline{v}_{\mathrm{d,q}} \underline{i}_{\mathrm{d,q}} - K_{\mathrm{T}} \underline{v}^{0}_{\mathrm{d,q}} \underline{i}^{0}_{\mathrm{d,q}} \tag{17}$$

The sum of the extra magnetic loss terms, i.e. $\Delta P_{\mathrm{fer}}$ and $\Delta P_{\mathrm{PM}}$, can be considered as the ratio between the mechanical power of the scaled and reference machine, as shown below:

$$\Delta P_{\mathrm{fer}} + \Delta P_{\mathrm{PM}} = T_{\mathrm{sh}} \Omega_{\mathrm{tr}} - K_{\mathrm{T}} T^{0}_{\mathrm{sh}} \Omega^{0}_{\mathrm{tr}} \tag{18}$$

### 3.5. *Scalable control scheme of PMSM*

One of the main advantages of EMR is to systematically deduce the control scheme based on the inversion rules [7]. These rules are used to deduce a scalable control scheme of PMSM, illustrated in the lower part of Fig. 2. The local control aims to track the torque setpoint of the PMSM $T^{*}_{\mathrm{sh}}$through d,q voltages $\underline{v}^{*}_{\mathrm{d,q}}$. The mechanical PA element (10) is first inverted by (19). Next, the Field-Oriented Control (FOC) technique (21) is used for the control of the reference PMSM. For this, two PI controllers $\underline{C_I}$ are utilized to track the d,q currents (22). Finally, equation (7) of the electrical power adaptation element is inverted to determine the scaled d,q voltages using (23).

$$T^{0*}_{\mathrm{sh}} = \frac{T^{*}_{\mathrm{sh}}}{K_{\mathrm{T}}} + \Delta T \tag{19}$$

$$T^{0*}_{\mathrm{em}} = T^{0*}_{\mathrm{sh}} + T^{0}_{\mathrm{fer}} + T^{0}_{\mathrm{PM}} \tag{20}$$

$$i^{0*}_{q} = \frac{T^{0*}_{\mathrm{em}}}{N_{\mathrm{p}} \left[ \psi^{0}_{\mathrm{magd}} + \left( L^{0}_{\mathrm{d}} - L^{0}_{\mathrm{q}} \right) i^{0*}_{\mathrm{d}} \right]} \tag{21}$$

$$\underline{v}^{0*}_{\mathrm{d,q}} = \underline{C_I} \left( \underline{i}^{0*}_{\mathrm{d,q}} - \underline{i}^{0\prime}_{\mathrm{d,q}} \right) + \underline{e}^{0\prime}_{\mathrm{d,q}} \tag{22}$$

$$\underline{v}^{*}_{\mathrm{d,q}} = K_{\mathrm{v}} \left( \underline{v}^{0*}_{\mathrm{d,q}} + \Delta R^{0} \underline{i}^{0\prime}_{\mathrm{d,q}} \right) \tag{23}$$

in which the superscript * refers to the control variables, $N_{\mathrm{p}}$ is the number of pole pairs, $L^{0}_{\mathrm{d}}$, and $L^{0}_{\mathrm{q}}$ are the inductances within the dq frame, and $\psi^{0}_{\mathrm{magd}}$ denotes the flux linkage of the magnet.

The new model organization of the scaled machine offers the possibility of employing the same control for the reference PMSM. The control structure of the reference machine remains the same, including the current controllers and their parameters. Only input and output are scaled. Therefore, various types of scaled machines can be rapidly tested by using EMR-based scaling laws.

## 4. STUDY CASE OF AN ELECTRIC VEHICLE

The reference machine used in this study is a traction interior PMSM, with a maximal power of 80 kW, a maximal torque of 280 Nm, and a base speed of 2728 rpm. The main geometrical parameters can be consulted in [8]. This reference machine is upscaled with a factor of 1.375 to improve the acceleration time from 0 to 100 km/h of an electric vehicle. The scaled PMSM is then connected to a mechanical source, denoted "Tract" (traction part) in Fig. 2. A classical model is used to detail the vehicle dynamics. The reader can refer to [9] for further information regarding the model and EMR of the mechanical part. Since the study concerns the PMSM, the electrical source ("Park" in Fig. 2) is considered ideal, i.e. the voltages applied to the PMSM model equal their references without any delay. For the analysis, the Artemis urban driving cycle is herein considered, which consists of a distance of 4.87 km with a maximal speed of 57.3 km/h. Using the speed profile, powertrain model, and vehicle data, the required torque and speed for the scaled PMSM can be determined, as shown in Figure 4.

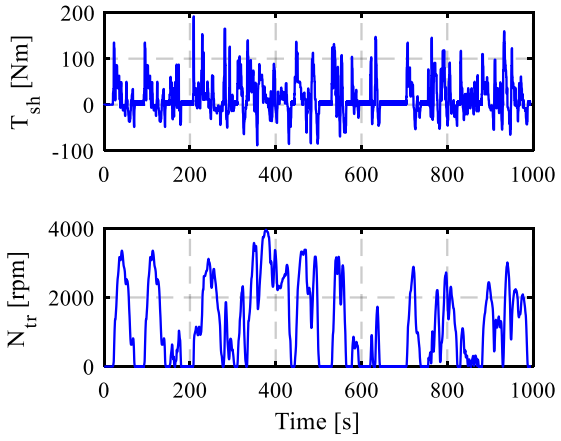


Figure 3: Torque (top) and speed (bottom) requested for the scaled PMSM with an Artemis urban driving cycle

Table 3: Electric vehicle parameters

| parameter | value |
|---|---|
| final drive ratio | 8.19 |
| drivetrain efficiency | 0.97 |
| wheels radius [m] | 0.316 |
| curb mass [kg] | 1505 |
| drag area [$m^2$] | 2.35 |
| rolling coefficient | 0.02 |
| reference acceleration time [s] | 10.1 |
| improved acceleration time [s] | 7.1 |

For the analysis, two scaled designs are considered as illustrative cases, and their respective scaling factors are summarized in Table 4. Note that the rewinding scaling factor $K_{\mathrm{W}}$ is adjusted to keep the same DC bus voltage rating of the scaled machine as the reference machine.

Table 4: an overview of scaling factors for the scaled designs

| Scaling choice | Scaled design 1 ($K_{\mathrm{T}}/K_{\mathrm{A}}/K_{\mathrm{R}}/K_{\mathrm{W}}$) | Scaled design 2 ($K_{\mathrm{T}}/K_{\mathrm{A}}/K_{\mathrm{R}}/K_{\mathrm{W}}$) |
|---|---|---|
| $B\sim1$ | 1.375 / 1 / 1.17 / 0.85 | 1.375 / 1.5 / 0.96 / 0.7 |
| $\Theta\sim1$ | 1.375 / 1 / 1.17 / 0.92 | 1.375 / 1.5 / 0.96 / 0.68 |
| Hybrid choice | 1.375 / 1 / 1.14 / 0.88 | 1.375 / 1.5 / 0.97 / 0.69 |

By consulting Fig. 4, it can be seen that the dissipated energy loss over the studied driving cycles differs according to the scaling choices and the selected scaling factors. For instance, the scaling choice $B\sim1$ using an axial scaling factor $K_{\mathrm{A}}$ of 1 results in the lowest dissipated loss energy when compared to the other scaling choices. However, when $K_{\mathrm{A}}$ is increased to 1.5, the last scaling choice leads to the highest energy consumption. This is mainly attributed to higher copper loss, as shown in Fig. 4. Conversely, for a $K_{\mathrm{A}}$ of 1.5, the hybrid choice results in the lowest dissipated energy.

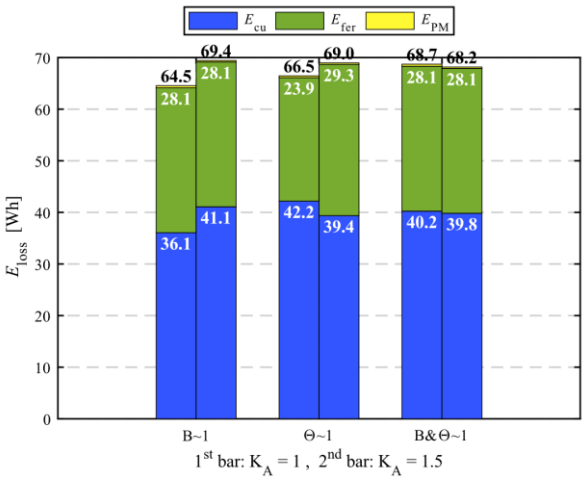


Fig. 4: Energy loss split between copper $E_{\mathrm{cu}}$, magnet $E_{\mathrm{mag}}$, and core iron $E_{\mathrm{fer}}$ during the Artemis urban driving cycle for the three scaling choices. Overall energy loss is shown in black.

For further analysis, Fig. 5 examines the equivalent loss terms $\Delta P$, presented in Section 4.3. Recall that the extra copper $\Delta P_{\mathrm{cu}}$, iron $\Delta P_{\mathrm{fer}}$ and magnet $\Delta P_{\mathrm{PM}}$ losses are incorporated in the electrical and mechanical power adaptation elements of the EMR-based scaling laws of the PMSM. For the first scaled design ($K_{\mathrm{A}} = 1$), the reduction in copper losses ($\Delta E_{\mathrm{cu}} < 0$) is greater for $B\sim1$ than the two other scaling choices. However, the choice $\Theta\sim1$ results in more reduction of the copper loss for $K_{\mathrm{A}} = 1.5$. This explains, the results obtained for the scaled copper loss, obtained in Fig. 4. Regarding the iron loss, $\Theta\sim1$ offers more reduction in the iron loss during the scaling process for $K_{\mathrm{A}}$ of 1 as compared to the other choices, while the opposite is observed for the second scaled design, resulting in increased iron losses. The $\Delta E_{\mathrm{fer}}$ is zero for $B\sim1$ as the iron loss linearly evolve with the torque scaling factor. Finally, the equivalent magnet $\Delta P_{\mathrm{PM}}$ is negligeable for the three scaling choices.

## 5. Conclusion

This paper sets new structuration of the scaling laws equations for ease of incorporation at system-level simulations. The methodology consists to keep the reference machine model unchanged but complemented with two electrical and mechanical power adaptation elements. The equations behind the electrical power adaptation element are herein derived for three different scaling choices: preserving magnetic field density, maintaining the temperature rise in the windings, and a hybrid choice of the last two ones. The methodology is demonstrated by a simulation of an electric vehicle, allowing a fast examination of the scaled losses for different scaled designs with a power scaling factor of 1.375. The simulation results for an urban driving cycle show that the scaling choice based on maintaining the magnetic field density results in the lowest energy consumption for an axial scaling factor of 1, while the hybrid choice shows better results for an axial scaling factor of 1.5. Further investigations will consider including a scalable model for the voltage source inverter following the energetic macroscopic representation-based scaling laws.

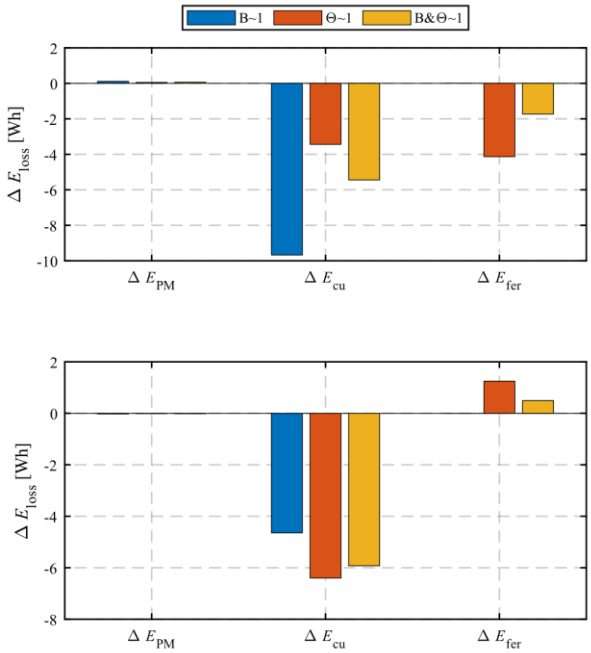


Fig. 5: Energy split in extra copper $\Delta E_{\mathrm{cu}}$, iron $\Delta E_{\mathrm{fer}}$, and magnet $\Delta E_{\mathrm{PM}}$ losses during the Artemis urban driving cycle, for axial scaling $K_A$ =1 (top), and $K_A$= 1.5 (down)

## 6. Acknowledgments

This study was supported by the French government through the Programme Investissement d'Avenir (I-SITE ULNE / ANR- 16-IDEX-0004 ULNE) managed by the "Agence Nationale de la Recherche", within the CUMIN-STeVE project.

## 7. References

[1] C. Liu, K. T. Chau, C. H. T. Lee, and Z. Song, "A Critical Review of Advanced Electric Machines and Control Strategies for Electric Vehicles," *Proc. IEEE*, vol. 109, no. 6, pp. 1004–1028, Jun. 2021, doi: 10.1109/JPROC.2020.3041417.

[2] P. Boscariol and D. Richiedei, “Energy optimal design of servo-actuated systems: A concurrent approach based on scaling rules,” *Renewable and Sustainable Energy Reviews*, vol. 156, p. 111923, Mar. 2022, doi: 10.1016/j.rser.2021.111923.

[3] S. Stipetic, D. Zarko, and M. Popescu, “Ultra-fast axial and radial scaling of synchronous permanent magnet machines,” *IET Electric Power Applications*, vol. 10, no. 7, pp. 658–666, Aug. 2016, doi: 10.1049/iet-epa.2016.0014.

[4] A. Borisavljevic, H. Polinder, and J. A. Ferreira, “On the Speed Limits of Permanent-Magnet Machines,” *IEEE Trans. Ind. Electron.*, vol. 57, no. 1, pp. 220–227, Jan. 2010, doi: 10.1109/TIE.2009.2030762.

[5] -Bernard -Multon, “Comparaison du couple massique de diverses architectures de machines tournantes synchrones à aimants,” *R.E.E.*, vol., no. 07, p. 85, 2006, doi: 10.3845/ree.2006.064, text in French.

[6] W. Lhomme, F. Verbelen, M. N. Ibrahim, and K. Stockman, “Energetic Macroscopic Representation of Scalable PMSM for Electric Vehicles,” in *2020 IEEE Vehicle Power and Propulsion Conference (VPPC)*, Gijon, Spain: IEEE, Nov. 2020, pp. 1–6. doi: 10.1109/VPPC49601.2020.9330981.

[7] A. Bouscayrol, J.-P. Hautier, and B. Lemaire-Semail, “Graphic Formalisms for the Control of Multi-Physical Energetic Systems: COG and EMR,” in *Systemic Design Methodologies for Electrical Energy Systems*, John Wiley & Sons, Ltd, 2012, pp. 89–124. doi: 10.1002/9781118569863.ch3.

[8] T. Burress, “Benchmarking State-of-the-Art Technologies,” *2013 U.S. DOE Hydrogen and Fuel Cells Program and Vehicle Technologies Program Annual Merit Review and Peer Evaluation Meeting*, p. 21, 2013.

[9] A. Desreveaux, A. Bouscayrol, R. Trigui, E. Hittinger, E. Castex, and G. M. Sirbu, “Accurate energy consumption for comparison of climate change impact of thermal and electric vehicles,” *Energy*, vol. 268, p. 126637, Apr. 2023, doi: 10.1016/j.energy.2023.126637.